Uncertainties on the $\overset{(-)}{\nu}_e/\overset{(-)}{\nu}_\mu$ and $\nu_e/\bar{\nu}_e$ cross-section ratio from the modelling of nuclear effects at 0.2 to 1.2 GeV neutrino energies and their impact on neutrino oscillation experiments

T. Dieminger,[1,*] S. Dolan,[2,†] D. Sgalaberna,[1,‡] A. Nikolakopoulos,[3]
T. Dealtry,[4] S. Bolognesi,[5] L. Pickering,[6] and A. Rubbia[1]

[1] *ETH Zurich, Institute for Particle physics and Astrophysics, CH-8093 Zurich, Switzerland.*
[2] *European Organization for Nuclear Research (CERN), 1211 Geneva 23, Switzerland.*
[3] *Theoretical Physics Department, Fermilab, Batavia IL 60510, USA.*
[4] *Lancaster University, Physics Department, Lancaster, United Kingdom.*
[5] *IRFU, CEA, Université Paris-Saclay, F-91191 Gif-sur-Yvette, France.*
[6] *Royal Holloway University of London, Department of Physics, Egham, Surrey, United Kingdom.*

Recent studies have demonstrated non-trivial behaviours in the cross-section extrapolation from ν_μ ($\bar{\nu}_\mu$) to ν_e ($\bar{\nu}_e$) interactions on nuclear targets in the charged-current quasi-elastic (CCQE) regime. In this article, the potential for mis-modeling of ν_μ/ν_e, $\bar{\nu}_\mu/\bar{\nu}_e$ and $\nu_e/\bar{\nu}_e$ cross section ratios due to nuclear effects is quantified by considering the model spread within the full kinematic phase space for CCQE interactions. Its impact is then propagated to a simulated experimental configuration based on the Hyper-K experiment, which is dominated by CCQE interactions. Although a relatively large discrepancy between theoretical models is confirmed for forward lepton angles at neutrino energies below 300 MeV and for a new region of phase space at lepton angles above 100°, both regions are demonstrated to contribute a very small portion of the Hyper-K (or T2K) flux integrated cross section. Overall, a systematic uncertainty on the oscillated flux-averaged $\nu_e/\bar{\nu}_e$ cross-section ratio is estimated to be ∼2%. A similar study was also conducted for the proposed lower-energy ESSνSB experiment configuration, where the resulting uncertainty was found to be larger.

I. INTRODUCTION

The currently-running accelerator-based long-baseline (LBL) neutrino experiments, T2K [1, 2] and NOvA [3, 4], are placing increasingly tight constraints on the parameters that describe neutrino oscillations within the three-flavour Pontecorvo–Maki–Nakagawa–Sakata (PMNS) framework [5]. Both experiments measure (anti)electron neutrino appearance ($\overset{(-)}{\nu}_\mu \to \overset{(-)}{\nu}_e$) as well as the (anti)muon neutrino disappearance (by inferring $\overset{(-)}{\nu}_\mu \to \overset{(-)}{\nu}_\mu$) in an (anti)muon neutrino beam at a detector placed a few hundred kilometres away from the neutrino beam production point, the far detector (FD). The oscillated electron and muon neutrino event rate distributions observed at the FD are compared with the unoscillated muon neutrino distributions observed at a near detector (ND), placed only a few hundred meters from where neutrinos are produced. For GeV-scale neutrino energies, such a configuration offers great sensitivity to the PMNS mixing parameters: θ_{23} (including the octant) and the complex phase δ_{CP}, responsible for the violation of the leptonic Charge-Parity (CP) symmetry within PMNS framework if $\sin\delta_{CP} \neq 0$. LBL experiments are also sensitive to one of the neutrino mass-squared splittings, Δm^2_{32}, and the neutrino mass ordering (MO), i.e. $\Delta m^2_{32} > 0$ (normal ordering, NO) or $\Delta m^2_{32} < 0$ (inverted ordering, IO) . Although the latest measurements performed by the T2K and NOvA experiments are still largely statistically limited, their sensitivity is continuing to improve as larger samples of data are collected in higher intensity neutrino beams [6]. The upcoming Hyper-K [7] and DUNE [8] experiments will aim to identify the correct neutrino MO and measure δ_{CP} with a resolution better than 20° to definitively confirm or rule out the possibility of a relatively large CP asymmetry within the PMNS three-flavor mixing framework. Another experiment, ESSνSB, has been proposed to further improve the resolution on δ_{CP} below 8° [9]. With approximately an order of magnitude more data than T2K and NOvA, the statistical uncertainty in the Hyper-K and DUNE experiments will be drastically reduced and systematic uncertainties due to the possible mis-modelling of the neutrino-nucleus interaction cross section will have a dominant impact on the accuracy and the resolution of measured neutrino oscillation parameters [10]. These uncertainties enter neutrino oscillation analyses in order to interpret event rate distributions, observed at the FD, in terms oscillation probabilities. For example, when neutrino interaction models are used to predict background rates or the smearing between true and observable neutrino energy, which is then used to infer the shape of the oscillation probability from observed interaction spectra. To reduce such uncertainties, current and future LBL experiments have intensive programs to deploy or develop increasingly performant near detectors [11–13].

Since the predominant sensitivity to δ_{CP} stems from an analysis of the difference of electron and antielectron

* Contact e-mail: tilld@ethz.ch
† Contact e-mail: Stephen.Joseph.Dolan@cern.ch
‡ Contact e-mail: davide.sgalaberna@cern.ch

neutrino appearance event rates at the FD, the uncertainty on the differences between the ND-constrained (anti)muon neutrino cross sections and the FD-relevant (anti)electron neutrino cross sections is especially important. In particular, the way these uncertainties propagate to the ratio of the electron to antielectron neutrino cross sections been shown to be a dominant uncertainty for analyses of δ_{CP} within both Hyper-K and DUNE [14, 15]. To ensure the experiments do not become prematurely limited by systematic uncertainties, this ratio should be understood at least at the 2%-3% level over the ranges of neutrino energies and interaction kinematics seen at their FD.

Assuming lepton universality, the only difference between charged-current muon and electron neutrino cross sections stems from the difference in the outgoing lepton mass. However, for interactions where the range of kinematically allowed energy and momentum transfers is comparable to lepton mass differences, physics processes which determine the cross section may do so differently for different flavours of neutrinos. In particular, previous works have investigated differences in the electron and muon neutrino cross sections due to the way nuclear effects change the impact of the restriction the lepton mass places on the allowed kinematic phase space.

In [16] the random phase approximation applied to a local Fermi gas (LFG-RPA) [17] was compared to continuum random phase approximation calculations for long-range nucleon correlations on top of Hartree-Fock nuclear ground state description (HF-CRPA) [18]. In general, the electron neutrino cross section may be expected to be larger than that of muon neutrinos because of wider kinematic phase space available due to the lower outgoing lepton mass (energy transfers closer to the available neutrino energy are allowed, and there is a corresponding broadening of permitted momentum transfer [19, 20]). However it was found that the trend is inverted at forward scattering angles for relatively small neutrino energies ($\lessapprox$ 500 MeV). An analysis of the impact of ground state modelling and RPA corrections on the the ratio of electron to muon neutrino total cross sections has also been shown in Ref. [21]. Here it is demonstrated that the difference in model predictions is small (<5%) for energies of interest of DUNE and T2K/Hyper-K.

A useful illustration of how nuclear ground state modelling and Pauli blocking can impact the ratio of electron to muon neutrino cross sections is given in [19]. The author demonstrates how low neutrino energies and forward scattering angles can conspire to make the available phase space for electron and muon neutrino cross sections very different for more restrictive nuclear ground state models. In particular a dramatic difference in the cross-section ratio is demonstrated for the low energy forward-angle case when a simple relativistic Fermi gas approach to Pauli blocking is or is not applied.

Finally, a detailed evaluation of the electron to muon cross-section ratio in CCQE processes at lepton angles below 60° was reported in [22] for interactions in carbon and argon. It was confirmed that taking into account a distortion of the final-state nucleon wavefunction, i.e. including final state interactions (FSI)[1], as well as Pauli blocking explains the dominance of muon neutrino over electron neutrino induced cross sections at forward angles. An analogous trend was found for both the HF-CRPA and the relativistic mean field approach (RMF) in [24].

Moreover, recent works have shown differences in the electron and muon neutrino cross sections due to radiative corrections rather than nuclear effects [25–27], which have been assigned a systematic uncertainty at the level of 2% at energies around one GeV [28]. The remainder of this article focuses only on differences in the cross sections due to nuclear effects.

Another important source of uncertainty stems from how differences in (anti)neutrino interactions between nuclear targets could alter the ratio of electron and muon neutrino cross sections. In fact, at the LBL experiments that deploy a water-based FD (oxygen and hydrogen target nuclei - H_2O), the ND complex typically also includes plastic scintillator detectors (carbon and hydrogen target nuclei - C_nH_n) that are not affected by high momentum thresholds (e.g. for protons) and can provide both precise particle tracking and calorimetry, and thus additional precious information for a precise characterisation of (anti)neutrino interactions. Therefore, the reduction of cross-section systematic uncertainties in the measurement of neutrino oscillations relies on the extrapolation from carbon to oxygen that must be under control. In the case of T2K, ratios between carbon and oxygen cross sections have been shown to differ substantially between models in the forward scattering region [29, 30], which is the same region of kinematic phase space muon and electron (anti)neutrino cross sections would be expected to differ the most.

In this article the impact of nuclear effects on the CCQE cross section ratios (ν_μ/ν_e, $\bar{\nu}_\mu/\bar{\nu}_e$, and $\nu_e/\bar{\nu}_e$) is studied. Interactions on oxygen nuclei (the dominant target for the T2K, Hyper-K and ESSνSB far detectors) are investigated across a variety of state-of-the-art and widely used models. Differences in the ratios between oxygen and carbon nuclei are also considered. The full phase space, rather than only forward lepton scattering, is investigated in detail and new features in the cross section ratios are identified.

A simple systematic uncertainty is derived to cover the observed model spread for the Hyper-K (which is also applicable to T2K, since they use the same neutrino beam) and ESSνSB experiments in the form of two normalisation factors with correlations, which together imply an

[1] Note that the "FSI" considered via the distortion of the outgoing nucleon wavefunction alters the *inclusive* cross section, in contrast to the usual application of intranuclear cascade FSI models within neutrino event generators. The relationship between these different approaches to modelling FSI is discussed in [23].

uncertainty on the ν_e versus $\bar{\nu}_e$ cross section ratio. For the T2K/Hyper-K neutrino flux, peaked at 0.6 GeV, this result can be directly compared with the normalisation systematic uncertainties currently used in LBL neutrino oscillation analyses [14, 28, 31, 32]. A systematic uncertainty that additionally accounts for the difference in the shape of the cross section ratios between models is left for future work as, in order to comprehensively evaluate the impact on searches for CP violation, more sophisticated analysis tools are necessary. It is worth noting that, for the case T2K and Hyper-K, a robust assessment of rate-based systematics considered here are most important for analyses focused on CP-violation discovery. However, systematic uncertainties on the shape become more important for accurately measuring CP-violating values of δ_{CP} in case of maximal CP violation or for determining the presence of small (but non-zero) CP-violation in the case of near CP conservation.

This work covers only CCQE interactions and so is not directly informative for the full energy spectra of the NOvA and DUNE experiments. It is also likely that analogous effects are applicable to the interaction channels more prevalent at higher energies, such as single pion production and multi-nucleon interactions, but an analogous analysis requires nuclear models for these channels at the same level of sophistication as exists for CCQE, which are not yet widely available.

II. ANALYSIS METHOD

CCQE neutrino interaction cross sections are generated with a flat incoming neutrino flux between 0 and 2 GeV on an oxygen target using the NEUT interaction event generator [33] setup to use either an LFG-RPA model (henceforth referred to as LFG for brevity) based on Ref. [34] and detailed in Ref. [35], or a model that uses the plane-wave impulse approximation using the Benhar spectral function (SF), based on Ref. [36]. Note that the axial mass parameter M_A^{QE}, which affects the normalisation and shape of the cross section, is set at NEUT's default values of 1.21 GeV for SF, and 1.05 GeV for LFG. The models are generated using NEUT's intranuclear cascade FSI model, but this does not affect the inclusive cross sections of interest in this work. The final simulations are processed using NUISANCE [37] for ease of use.

The NEUT cross-section predictions are compared to inclusive cross-section calculations using SuSAv2 [38] or a HF model with and without CRPA corrections, [18, 39] , produced using the hadron tensor tables prepared for their implementations within the GENIE event generator [29, 40, 41]. In the HF-CRPA case, the distortion of the outgoing nucleon wavefunction (i.e. FSI) can be enabled and disabled which, incontrast to intranuclear cascade FSI, does change the predicted inclusive cross sections. These give cross sections identical to those made using the full model calculation up to very small differences due to treatments of interpolation between the points calculated in the tables.

Together the considered models cover a wide range of approaches to accounting for nuclear effects and represent those most commonly used for neutrino oscillation analyses. The SF and LFG models are used in the latest T2K [2] and NOvA [4] analyses respectively (although it should be noted that NOvA uses the GENIE implementation of the model, which has some differences). The HF-CRPA model offers the opportunity to turn RPA and FSI effects on and off, the latter of which was found to be responsible for the large differences in muon and electron neutrino cross sections in Ref. [22], as discussed in section I. The SuSAv2 model acts as an inclusive extension of relativistic mean field calculations [24], which includes an alternative description of FSI and, as noted in section I, also produces electron to muon cross-section ratios with interesting trends. Neither SF nor LFG include FSI effects in the calculation of the inclusive cross section within NEUT. The SF model contains options to modify the Pauli blocking treatment, which has also been shown to be impactful in determining muon to electron cross-section ratios [19] as discussed in section I. The choice of the M_A^{QE} is also investigated as a source of uncertainty on the ratios. A summary of all the studied models is provided in table I.

Predictions of electron to muon neutrino and electron neutrino to antineutrino cross-section ratios as a function of neutrino energy and outgoing lepton angle are compared between models. The ratio of flux-averaged cross sections for T2K/Hyper-K and ESSνSB experiments are calculated. The relative difference of the ratios for each of the models is analysed, and taken as an estimation of the level of uncertainty on (anti)electron neutrino appearance event rates due to nuclear effects modifying the ratio with their muon neutrino counterparts. In an attempt to attribute the differences found to particular physics, ratios are re-calculated after systematically changing the modelling of nuclear and nucleon-level effects within the models (considering all those listed within table I.

The predictions of the SF and LFG models (and their variations) are subject to statistical uncertainties corresponding to the number of NEUT events generated. For each interaction model and neutrino flavour, 300 million NEUT events were generated. The impact of statistical uncertainties on the cross-section ratios of interest is detailed in appendix B. In general the uncertainties are very small ($\sim 1\%$ in the binning shown) and, since NEUT populates kinematic phase space in proportion to the predicted cross section, the regions of slightly larger statistical uncertainty are also those where oscillation experiments would not expect to be observing events. Note also that there are no statistical uncertainties on predictions from models other than LFG and SF, as these provide a direct calculation calculation of the cross section without any event generation.

Model	Description
SuSAv2	Model from [38]
HF	Model from [18] w/o CRPA corrections, w/ FSI
HF-CRPA	w/ CRPA corrections, w/ FSI
HF-CRPA PW	w/ CRPA corrections, w/o FSI
HF-CRPA C	w/ CRPA corrections, w/ FSI, carbon target
SF	Model from NEUT based on [36]
SF w/o PB	w/o Pauli blocking
SF M_A^{QE}1.03	w/ modified nucleon axial mass
LFG	Model from NEUT based on [34]

TABLE I: The list of CCQE cross-section models used in this work. All are calculated for an oxygen target nucleus unless otherwise specified. The same ordering of the models is used in fig. 5. Note that "FSI" refers to the consideration of a distortion of the outgoing nucleon wavefunction rather than the application of an nuclear cascade (which would not impact the studies shown).

III. RESULTS

A ratio between electron and muon neutrino differential cross sections, respectively $\frac{d\sigma^{\nu_e}}{d\cos\theta_e}$ and $\frac{d\sigma^{\nu_\mu}}{d\cos\theta_\mu}$, in a certain range of incoming neutrino energy (E_ν) and outgoing lepton angle with respect to the incoming neutrino (θ_e or θ_μ) is defined as:

$$R^{\text{Model}}_{\nu_e/\nu_\mu}(E_\nu,\theta_{lep}) = \left[\frac{d\sigma^{\nu_e}}{d\cos\theta_e}\Big/\frac{d\sigma^{\nu_\mu}}{d\cos\theta_\mu}\right]^{\text{Model}}(E_\nu,\theta_{lep}) \quad (1)$$

This is shown for the SF (including Pauli blocking) and HF-CRPA models in fig. 1. Large differences between the HF-CRPA and SF models are seen in the forward scattered region. This has been extensively studied within the HF-CRPA model in [22] and shows values of $R^{\text{HF-CRPA}}_{\nu_e/\nu_\mu} < 0.9$. Although this behaviour is also observed in SF, it is much weaker. Another region of the phase space showing obvious deviations from a unity ratio is observed in HF-CRPA for neutrino energies below 0.3 GeV. A similar feature is observed for SF for antineutrinos but not for neutrinos. It is worth noting that a relatively wide structure is observed for the case of antineutrinos at energies between 0.3 and 0.5 GeV and lepton angles in both models above >130°.

To better quantify these deviations, the double ratio of the differential cross section predicted by two different models is computed as:

$$RR^{\text{Model 1/Model 2}}_{\nu_e/\nu_\mu}(E_\nu,\theta_{lep}) = \frac{R^{\text{Model 1}}_{\nu_e/\nu_\mu}(E_\nu,\theta_{lep})}{R^{\text{Model 2}}_{\nu_e/\nu_\mu}(E_\nu,\theta_{lep})}. \quad (2)$$

The resulting distributions for neutrinos and antineutrinos, obtained by comparing HF-CRPA to SF, are shown in fig. 2. As expected, the forward scattered region at angles below 20 degrees show a large difference between the models. However, it is interesting to see that the differences remain non-negligible when considering angles larger than about 50° for the oscillation maximum energy (∼ 0.6 GeV). A region at angles larger than 100° also shows significant differences, which persist when comparing SF to any HF-based model.

A. Impact on oscillation experiments: Hyper-K

In order to quantify the impact of potential cross-section mismodelling, the contours highlighting the regions with large $RR^{\text{HF-CRPA/SF}}_{\nu_e/\nu_\mu}$ are extracted from fig. 2 and overlaid on expected oscillated ν_e and $\overline{\nu}_e$ appearance event distributions at T2K/Hyper-K in fig. 3. [2] Details of the simulation of the experimental configuration are given in appendix A. Note that the event rates are calculated using only CCQE interactions, without applying any efficiency corrections or detector smearing. From fig. 3 it is clear that neither the very large differences in the very forward region (¡20°) discussed in Ref. [22], nor the differences at low neutrino energies (¡0.3 Gev), will have any significant impact on T2K or Hyper-K oscillation analyses, as only a very small portion of CCQE interactions will fall within this region. However, it can also be seen that a sizeable fraction of the ν_e and $\bar{\nu}_e$ oscillated spectra fall in the higher angle region of the phase space where $RR^{\text{HF-CRPA/SF}}_{\nu_e/\nu_\mu}$ differs from unity by more than 2%.

As discussed in section I, the most critical systematic uncertainty in the measurement of δ_{CP}, the neutrino MO and the θ_{23} octant is the potential mis-modeling of the ν_e cross section with respect to the $\bar{\nu}_e$ one. Hence, the computed $RR^{\text{HF-CRPA/SF}}_{\nu_e/\bar{\nu}_e}$ is shown in fig. 4. It can be seen that the regions with the largest deviations from unity overlap only with the extreme tails of the expected event distribution (i.e. at very low interaction cross section). Such regions are approximately for neutrino energies either below 0.3 GeV or for outgoing lepton angles above 100° and neutrino energy below 0.8 GeV. In the case of antineutrino interactions, which have a larger portion of their cross section at more forward outgoing lepton angles, the overlap with regions of large deviations from unity is even smaller.

1. *Quantifying an uncertainty*

A broad estimate of the integrated uncertainty on the expected $\overset{(-)}{\nu}_e$ appearance event rates associated with differences between electron and muon neutrino cross sections due the modelling of nuclear effects for can be computed by averaging the model differences in fig. 2

[2] The event spectra were built with the oscillation parameters $\sin^2\theta_{12} = 0.297$, $\sin^2\theta_{13} = 0.0214$, $\sin^2\theta_{23} = 0.526$, $\Delta m^2_{21} = 7.37\times10^{-5}$, $\Delta m^2_{32} = 2.463\times10^{-3}$, $\Delta m^2_{32} > 0$, $\delta_{CP} = 0$. The SF model implemented in NEUT was used.

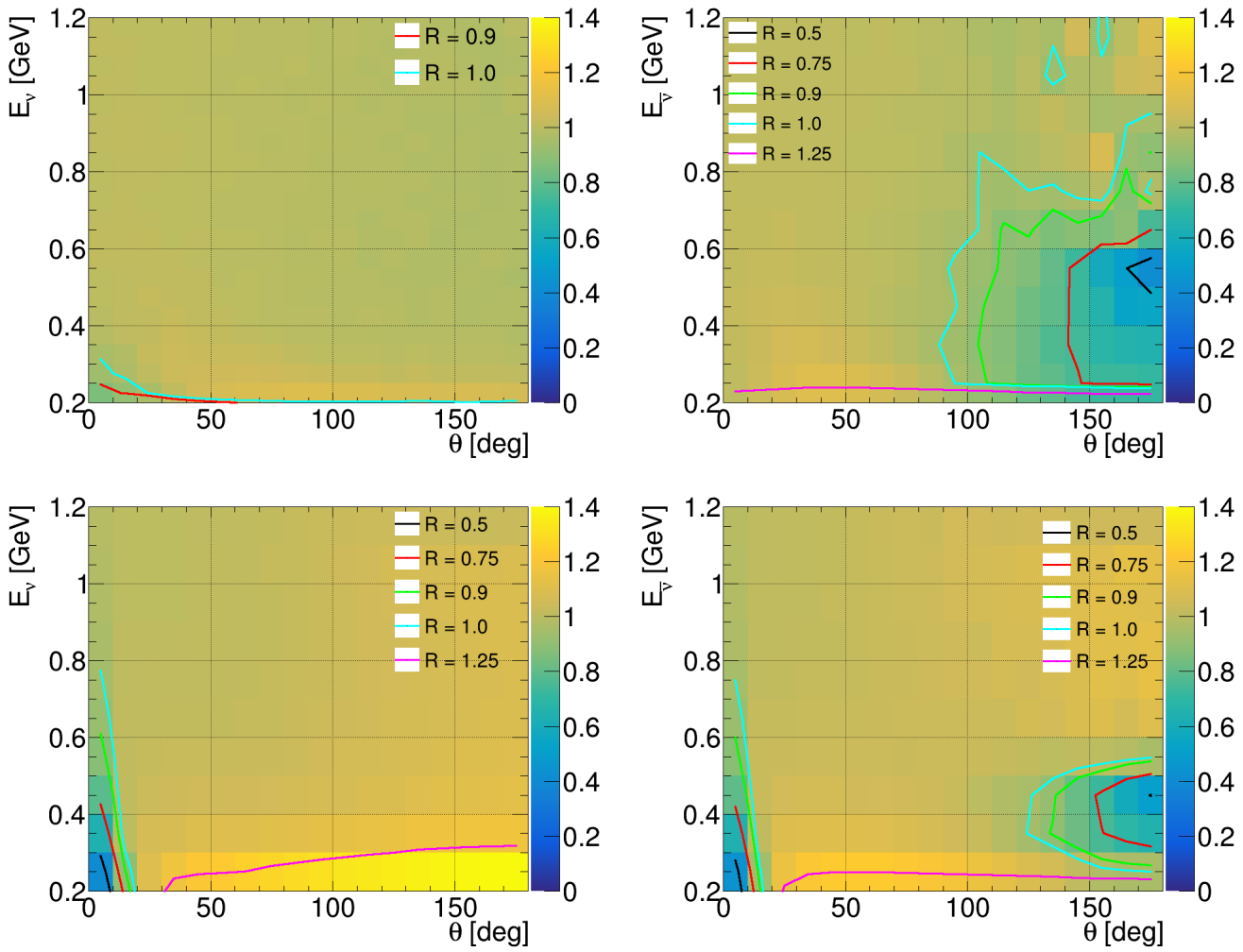

FIG. 1: The single ratios $R^{\mathrm{SF}}_{\nu_e/\nu_\mu}$ (top-left), $R^{\text{HF-CRPA}}_{\nu_e/\nu_\mu}$ (bottom left), $R^{\mathrm{SF}}_{\bar{\nu}_e/\bar{\nu}_\mu}$ (top-right) and $R^{\text{HF-CRPA}}_{\bar{\nu}_e/\bar{\nu}_\mu}$ (bottom-right) are shown. The X and Y axes show respectively the outgoing lepton angle and the neutrino energy. The contour lines highlight the regions where the single ratio significantly deviates from unity and are built using a bi-linear interpolation based on the four nearest bin centres [42]. Note that this uses unseen bins for neutrino energies less than 0.2 GeV.

over the neutrino and antineutrino event distributions predicted with the SF model shown in fig. 3. The uncertainties for electron neutrinos ($\Delta^{\text{Model 1/Model 2}}_{\nu_e/\nu_\mu}$) and antineutrinos ($\Delta^{\text{Model 1/Model 2}}_{\bar{\nu}_e/\bar{\nu}_\mu}$) are defined respectively as $|RR^{\text{Model 1/Model 2}}_{\nu_e/\nu_\mu} - 1|$ and $|RR^{\text{Model 1/Model 2}}_{\bar{\nu}_e/\bar{\nu}_\mu} - 1|$. They both can be either fully correlated or fully anti-correlated depending on whether the averaged model differences cause the cross section ratios, $RR^{\text{HF-CRPA/SF}}_{\nu_e/\nu_\mu}$ and $RR^{\text{HF-CRPA/SF}}_{\bar{\nu}_e/\bar{\nu}_\mu}$, to change in the same or the opposite direction. They are computed as:

$$\Delta_{\nu_e/\bar{\nu}_e} = \sqrt{\Delta^2_{\nu_e/\nu_\mu} + \Delta^2_{\bar{\nu}_e/\bar{\nu}_\mu} - 2C\Delta_{\nu_e/\nu_\mu}\Delta_{\bar{\nu}_e/\bar{\nu}_\mu}}, \quad (3)$$

where C is determined from the aforementioned correlation between Δ_{ν_e/ν_μ} and $\Delta_{\bar{\nu}_e/\bar{\nu}_\mu}$ (1 for correlated, -1 for anti-correlated). For instance, the result of this uncertainty calculation exercise for the SF and HF-CRPA model is $\Delta^{\text{HF-CRPA/SF}}_{\nu_e/\nu_\mu} = 2.9\%$, $\Delta^{\text{HF-CRPA/SF}}_{\bar{\nu}_e/\bar{\nu}_\mu} = 1.3\%$ and $\Delta^{\text{HF-CRPA/SF}}_{\nu_e/\bar{\nu}_e} = 1.6\%$.

From the analysis of the uncertainties on $RR^{\text{HF-CRPA/SF}}_{\nu_e/\nu_\mu}$ and $RR^{\text{HF-CRPA/SF}}_{\bar{\nu}_e/\bar{\nu}_\mu}$ in fig. 2, it is not surprising that the uncertainty in the neutrino cross-section ratio is larger than the one for the antineutrinos, as the more forward anti-neutrino cross section overlaps less with the region of cross-section ratios that differ significantly from unity.

The flux-averaged uncertainties derived for comparisons of each pair of models introduced in section II and table I are shown as a matrix in fig. 5. As different models predict different (anti)neutrino event distributions, a

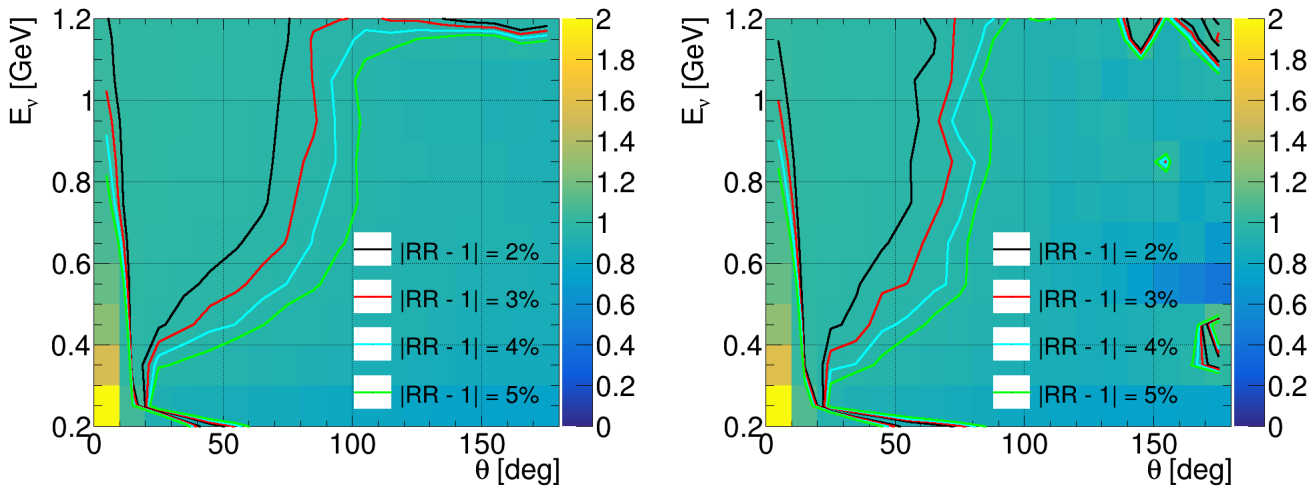

FIG. 2: The neutrino (left), $RR^{\text{HF-CRPA/SF}}_{\nu_e/\nu_\mu}$, and antineutrino (right), $RR^{\text{HF-CRPA/SF}}_{\bar{\nu}_e/\bar{\nu}_\mu}$, are shown. The X and Y axes show respectively the outgoing lepton angle and the neutrino energy. The different contour lines highlight the regions where $|RR^{\text{HF-CRPA/SF}}_{\nu_e/\nu_\mu} - 1| > 0.02$ (black), 0.03 (red), 0.04 (blue), 0.05 (green). These are built using a bi-linear interpolation based on the four nearest bin centres [42]. Note that this uses unseen bins for neutrino energies less than 0.2 GeV.

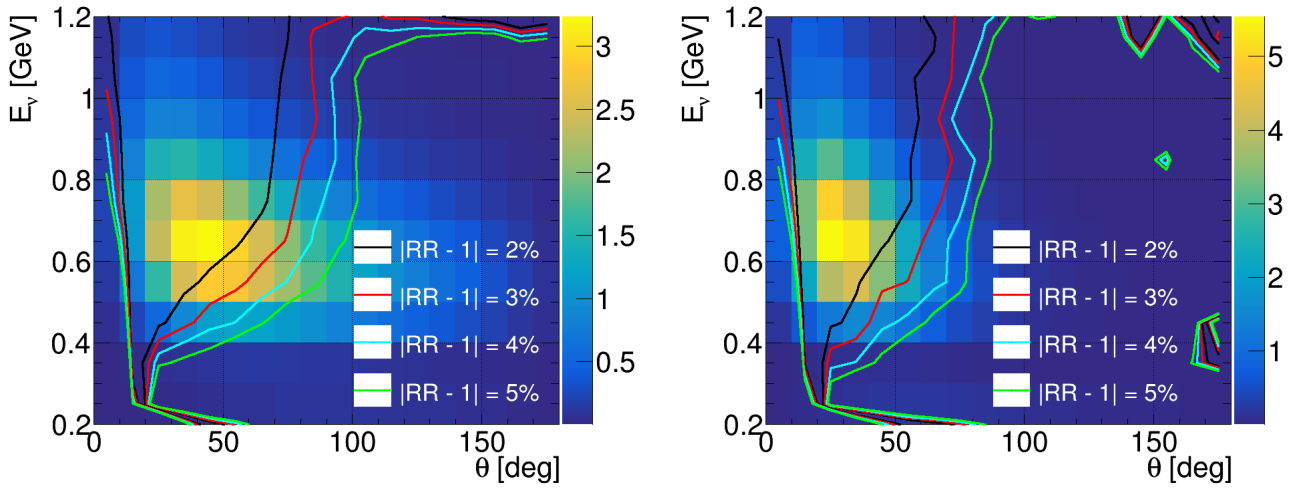

FIG. 3: The contour lines that highlight the regions where $|RR^{\text{HF-CRPA/SF}}_{\nu_e/\nu_\mu} - 1| > 0.02$ (black), 0.03 (red), 0.04 (blue), 0.05 (green) are taken from fig. 2 and overlaid on the oscillated ν_e (left) and $\overset{(-)}{\nu}_e$ (right) events expected at the far detector built using the SF model. The X and Y axes show respectively the outgoing lepton angle and the neutrino energy. The Z-axis shows the relative proportion of the event rate in each bin as a percentage.

pair of systematic uncertainty was obtained by averaging over the event rates predicted by both models. Hence, the lower triangle in fig. 5 is averaged over the event rate distribution predicted by the model given on the x-axis, while the upper triangle contains the resulting values from the averaging over the model on the y-axis, resulting in an asymmetric matrix. This pairwise comparison derived from different model combinations permits an analysis of the possible physical source of differences in predictions of R_{ν_e/ν_μ} and $R_{\bar{\nu_e}/\bar{\nu_\mu}}$, which is the subject of the following subsection.

2. *Investigating the source of the nuclear model uncertainties*

As discussed in section I, the cause of differences in model predictions of the electron to muon neutrino cross-

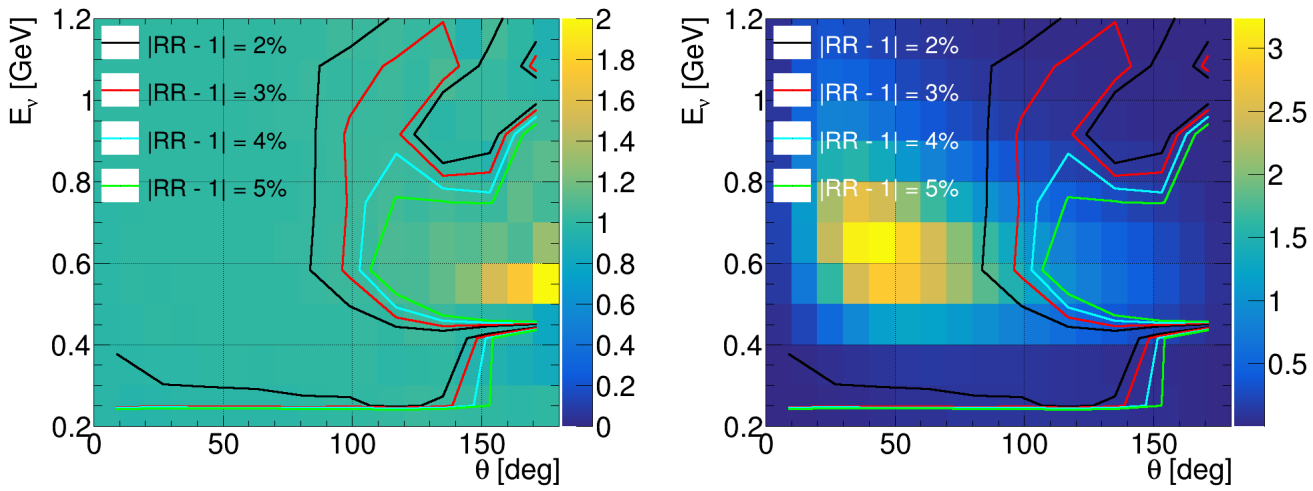

FIG. 4: On the left, the $RR^{\text{HF-CRPA/SF}}_{\nu_e/\bar{\nu}_e}$ is shown. The different contour lines highlight the regions where $|RR^{\text{HF-CRPA/SF}}_{\nu_e/\bar{\nu}_e} - 1| > 0.02$ (black), 0.03 (red), 0.04 (blue), 0.05 (green). On the right, the oscillated ν_e events expected at the far detector built using the SF model is shown with the $RR^{\text{HF-CRPA/SF}}_{\nu_e/\bar{\nu}_e}$ contour lines (which are the same as in left figure) overlaid. The Z-axis of the right plot shows the relative proportion of the event rate in each bin as a percentage. The X and Y axes show respectively the outgoing lepton angle and the neutrino energy.

section ratio has previously been assigned to a number of physical processes. In this section the uncertainty calculation is repeated for a variety of model pairs containing systematically different physics in an attempt to establish underlying sources of the uncertainty related to:

1. the variation of the nucleon axial mass, M_A^{QE};
2. Pauli blocking;
3. CRPA corrections for long-range nucleon correlations;
4. final state interactions;
5. different nuclear ground-state models.

In general, the largest discrepancy can be seen between the HF or RMF based models and the rest of the tested models.

Influence of M_A^{QE}***:*** The nominal values of M_A^{QE} in the HF-CRPA and SF models are 1.03 and 1.21 GeV respectively. The impact of changing M_A^{QE} to 1.03 GeV in SF, broadly spanning the range of values implied by cross-section measurements [43], is investigated as a source of uncertainty. The uncertainties introduced in section III A 1 are calculated between SF with the two different values of M_A^{QE}. The resulting uncertainties are negligible (less than 0.1%) for every metric considered (Δ_{ν_e/ν_μ}, $\Delta_{\bar{\nu}_e/\bar{\nu}_\mu}$, $\Delta_{\nu_e/\bar{\nu}_e}$).

Pauli blocking: Pauli blocking introduces a region at small angles and low energies where, counter intuitively, the muon neutrino cross section becomes larger than the electron neutrino cross section, as discussed in section I and described in [19, 22]. In order to investigate the influence of Pauli blocking the nominal SF model is compared to a version in which the Pauli blocking was disabled. The resulting systematic uncertainties for all metrics considered due to turning Pauli blocking on and off in the SF model is at the level of 0.2% or less. This small impact is because Pauli blocking affects a very narrow region of kinematic phase space which contains only a very small portion of the total cross section. Additional analysis of the impact of Pauli blocking on the SF cross section predictions is provided in appendix C.

Inclusion of CRPA nucleon correlations: As discussed in section I, the HF-CRPA model is based on a mean-field HF approach with CRPA corrections to model long-range nuclear correlations. The influence of these corrections on the derived uncertainties is calculated as in the previous paragraphs. Overall their inclusion leads to an uncertainty of less than 0.2% for all metrics.

Final State Interactions: A major difference between the HF-CRPA and SF models is the inclusion of FSI in the calculation of the inclusive cross section, as described in section I. This was identified as part of the cause of the HF-CRPA forward scattering features shown in fig. 1 [22]. The impact of FSI was studied

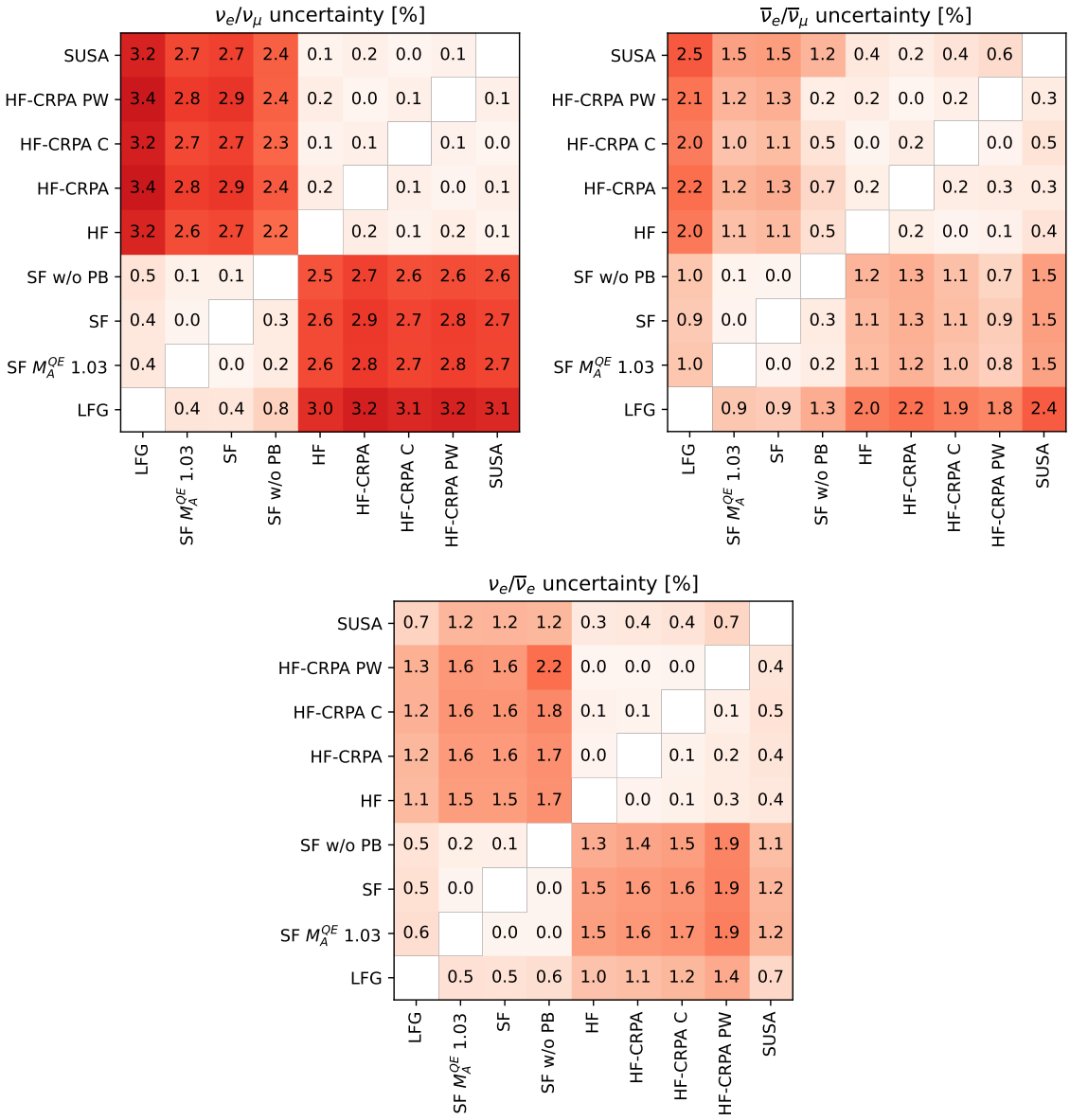

FIG. 5: The flux-average uncertainties in percent obtained by comparing different cross section models Δ_{ν_e/ν_μ} (top left), $\Delta_{\bar{\nu}_e/\bar{\nu}_\mu}$ (top right), $\Delta_{\nu_e/\bar{\nu}_e}$ (bottom). The details of the models labelled on the X and Y axes are provided in table I. The lower triangle is averaged over the event rate distribution predicted by the model given on the x-axis, while the upper triangle contains the resulting values from the averaging over the model on the y-axis, resulting in an asymmetric matrix.

within the HF-CRPA model by turning its effects on and off, as stated in section II. The derived uncertainty was found to be less than 0.3%, for all metrics. This is due to the small overlap between the heavily impacted forward lepton region and the phase space covered by the electron (anti)neutrino appearance events expected at the Hyper-K (or T2K) FD.

Nuclear model: Rather than comparing HF-CRPA with SF, uncertainites are instead derived from comparing the predictions of the NEUT-generated LFG model and the calculated SuSAv2 model to the SF model. The results in fig. 5 show that SuSAv2 and LFG lie somewhere between the SF and HF(-CRPA). The result of SuSAv2 is closer to the HF(-CRPA) one, which also uses a mean-field nuclear model with similar behaviour at intermediate interaction kinematics. This clustering of models highlights that the largest discrepancies are likely given by the different the nuclear models, in particular of the nuclear ground state (since FSI and Pauli blocking effects individually were not large). Whilst the difference in $^{(-)}\nu_e/^{(-)}\nu_\mu$ cross section ratios between

models is dominated by the very forward and backward regions, as highlighted for the SF and HF-CRPA case in fig. 2, the impact on Hyper-K oscillated ν_e and $\bar{\nu}_e$ event rates remains driven by differences at intermediate scattering angles.

3. *Investigating the uncertainty related to differences between carbon and oxygen nuclear models*

As described in section I, it is important to study the uncertainty related to potentially large differences in the modelling of (anti)neutrino interactions in oxygen and carbon target nuclei. In order to evaluate this, the cross-section calculation from HF-CRPA on carbon nucleus was compared with cross-section calculations using an oxygen target. $R^{\text{HF-CRPA }^{12}C}_{\nu_e/\nu_\mu}$ and $R^{\text{HF-CRPA }^{12}C}_{\bar{\nu}_e/\bar{\nu}_\mu}$ were studied and the related uncertainty was evaluated from the double ratio defined in eq. (2), following the same procedure described in section II.

The resulting uncertainty on the $\nu_e/\overline{\nu}_e$ cross section ratio is comparable to the one obtained when comparing only models on carbon nucleus, suggesting that carbon-to-oxygen differences appears to have a subdominant effect on the cross-section ratios, at least for the HF-CRPA model.

4. *Impact on the oscillated event rate*

As discussed in section I, the sensitivity to δ_{CP} and the neutrino MO is achieved by precisely measuring and comparing the $\nu_\mu \to \nu_e$ and the $\overline{\nu}_\mu \to \overline{\nu}_e$ oscillation probabilities. Both the search for leptonic CP symmetry violation and the definition of the neutrino MO rely on the precise measurement of an asymmetry between the $\nu_\mu \to \nu_e$ and $\bar{\nu}_\mu \to \bar{\nu}_e$ appearance probabilities. To better visualise such effect and compare it with the uncertainties Δ_{ν_e/ν_μ}, $\Delta_{\bar{\nu}_e/\bar{\nu}_\mu}$ and $\Delta_{\nu_e/\bar{\nu}_e}$ derived in section III A 1, "bi-event" plots were produced. These show the expected number of $\nu_\mu \to \nu_e$ versus $\bar{\nu}_\mu \to \overline{\nu}_e$ appearance events detected at the FD for different values of the oscillation parameters. The simulation of the Hyper-K experimental configuration is detailed in appendix A.

The bi-event plots are shown for different values of δ_{CP}, the MO and $\sin^2\theta_{23}$ in fig. 6. Each point in the bi-event ellipse corresponds to a different oscillation model, i.e. a different set of values of the oscillation parameters. The separation between different oscillation models is compared with the statistical uncertainty as well as the cross-section uncertainty derived from the model spread outlined in the previous sections. Whilst the largest discrepancy between any pair of models for $RR_{\nu_e/\bar{\nu}_e}$ is $\Delta^{(\text{HF-CRPA PW}) \text{ / } (\text{SF w/o PB})}_{\nu_e/\overline{\nu}_e} = 2.2\%$, note that this is a comparison of incomplete models (the former without FSI and the latter without Pauli Blocking). Therefore, as the complete models in their nominal configuration showing the largest differences in the predictions of $RR_{\nu_e/\bar{\nu}_e}$, differences between HF-CRPA and SF are used for the uncertainty calculation.

It can immediately be noted that the uncertainty Δ_{ν_e/ν_μ} is slightly larger than $\Delta_{\bar{\nu}_e/\bar{\nu}_\mu}$ and so the cross-section modelling uncertainty bar shows a slope steeper than 45°. It can also be observed that the impact of the normalisation uncertainties, Δ_{ν_e/ν_μ} and $\Delta_{\bar{\nu}_e/\bar{\nu}_\mu}$, associated with the modelling of nuclear effects are comparable to the statistical uncertainty but are fully correlated. Hence, the resulting uncertainty mostly affects the sensitivity to the CP conserving term (proportional to $\cos\delta_{CP}$) of the oscillation probability, rather than the CP violating one (proportional to $\sin\delta_{CP}$). More specifically, it introduces a degeneracy between the CP conserving values $\delta_{CP} = 0$ and π, rather than between $\delta_{CP} = \pm\pi/2$ (CP violating) and 0, π (CP conserving)[3]. Moreover, it does not extend the range of δ_{CP} values for which there is degeneracy between the different MO and δ_{CP} but it does enhance the existing significant degeneracy in regions where the ellipses for the different MO overlap.

Fig. 6 also shows that a stronger degeneracy is introduced in the measurement of $\sin^2\theta_{23}$, whose effect is correlated between ν_e and $\overline{\nu}_e$ events. In particular, the cross-section modelling uncertainty $\Delta_{\nu_e/\bar{\nu}_e}$ can therefore affect the determination of the θ_{23} octant, which only can be resolved with $\nu_\mu \to \nu_e$ and $\bar{\nu}_\mu \to \bar{\nu}_e$ measurements.

B. Impact on oscillation experiments: ESSνSB

A sensitivity study analogous to the one in section III has been conducted for a configuration similar to the ESSνSB conceptual experiment [9] using an FD baseline of 360 km. The (anti)neutrino flux is peaked around 0.3 GeV, compared to Hyper-K's 0.6 GeV. Therefore, it is expected that the ESSνSB may be subject to larger uncertainties related to a potential mismodeling of the $\nu_e/\bar{\nu}_e$ cross section ratio. Details of the simulation of an ESSνSB-like configuration can be found in appendix A. The largest deviation of $RR_{\nu_e/\bar{\nu}_e}$ from unity was found from the comparison of the SF and the HF-CRPA models, resulting in $\Delta_{\nu_e/\nu_\mu} = 6.4\%$, $\Delta_{\overline{\nu}_e/\overline{\nu}_\mu} = 2.2\%$ and $\Delta_{\nu_e/\overline{\nu}_e} = 4.2\%$, considerably larger than the uncertainties derived from the Hyper-K simulation.

Bi-event plots were generated following the same procedure used in section III A 4. The results are shown in fig. 7. Features analogous to those described for the Hyper-K case can be observed, i.e. the degeneracy is mostly introduced between CP conserving values of δ_{CP}, rather than CP violating ones. Moreover, the impact

[3] For reference, an approximated parametrization of the neutrino oscillation probability can be found in [44].

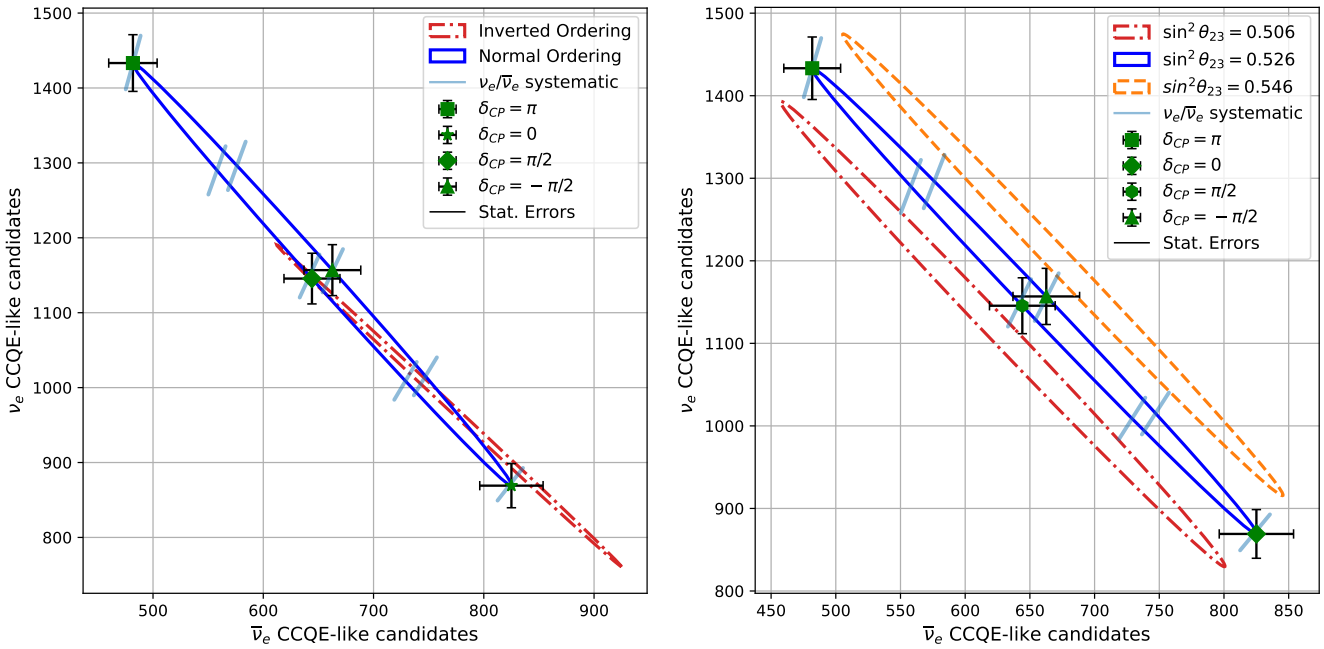

FIG. 6: The bi-event ellipse plots are shown for for the Hyper-K experiment. Left: bi-event ellipse for NO (blue solid line) and IO (red dashed line) and different values of δ_{CP}. Right: bi-event ellipse $\sin^2\theta_{23} = 0.506$ (red dashed line), 0.526 (blue solid line), 0.546 (orange dashed line) and δ_{CP}. The green dots highlight different values of δ_{CP} and the black bars show the corresponding statistical uncertainty. The diagonal light blue bar shows the modelling uncertainty on the $\nu_e/\bar{\nu}_e$ ($\Delta^{HF-CRPA/SF}_{\nu_e/\bar{\nu}_e}$).

of the estimated systematic uncertainty is found to be much larger than the projected statistical uncertainties and significantly impact the sensitivity to determining the $\sin^2\theta_{23}$ octant.

It is worth noting that the ESSνSB experimental concept shows sensitivity to both the first and the second oscillation maxima, as shown in fig. 8. Hence, the energy spectral information becomes more relevant than for the Hyper-K case, making the bi-event plot based sensitivity study more limited compared to an oscillation analysis that also includes shape information.

IV. SUMMARY AND OUTLOOK

In this article we analysed and quantified the impact of potential mismodelling of the ν_e/ν_μ and $\bar{\nu}_e/\bar{\nu}_\mu$ cross-section ratios due to nuclear effects on measurements of the neutrino oscillation probability at future LBL experiments. Whilst fig. 1 and fig. 2 confirm large differences between nuclear model predictions of the ratio of muon and electron (anti)neutrino cross sections at both forward regions and (in the antineutrino case) at very high angles, as noted in previous works, fig. 3 shows that these are also regions of very low flux-averaged cross section for T2K/Hyper-K (whilst not shown explicitly, this is also the case for ESSνSB). Still, the ratio of model predictions for flux-averaged cross-section ratios of ν_e/ν_μ, $\bar{\nu}_e/\bar{\nu}_\mu$ and $\bar{\nu}_e/\bar{\nu}_\mu$ remains non-negligible relative to the few-% level of precision required by future generations of oscillation experiments.

For T2K and Hyper-K, model differences are equal or smaller than 2.2%, as summarised in fig. 5. For a Hyper-K-like simulation, it is shown that the uncertainties imply only a weak worsening of the sensitivity to the CP violating term ($\sin\delta_{CP}$) of the oscillation probability and neutrino MO but that a substantial impact, comparable to the one of statistical uncertainties, is expected for measurements of the CP conserving term ($\cos\delta_{CP}$) and the $\sin^2\theta_{23}$ octant. Similar conclusions are made for ESSνSB. However, the lower energy flux gives a systematic uncertainty from model spread of $RR_{\nu_e/\bar{\nu}_e}$ up to 4.3%, considerably larger than the expected statistical uncertainty. Since this analysis considered a spread of models which consider changes in only nuclear and nucleon structure, the derived uncertainties should be considered an addition to those associated with radiative corrections derived in other recent works [25–27].

Studies changing the various components of the underlying physics model (the nucleon axial mass, Pauli blocking, CRPA correlations and FSI modelling) were unable to identify any single cause of large model differences between HF-CRPA or SuSAv2 and SF or LFG. Fig. 5 highlights that the largest change to the ratios within a model is the role of FSI within HF-CRPA, but the difference between applying or not applying FSI remains

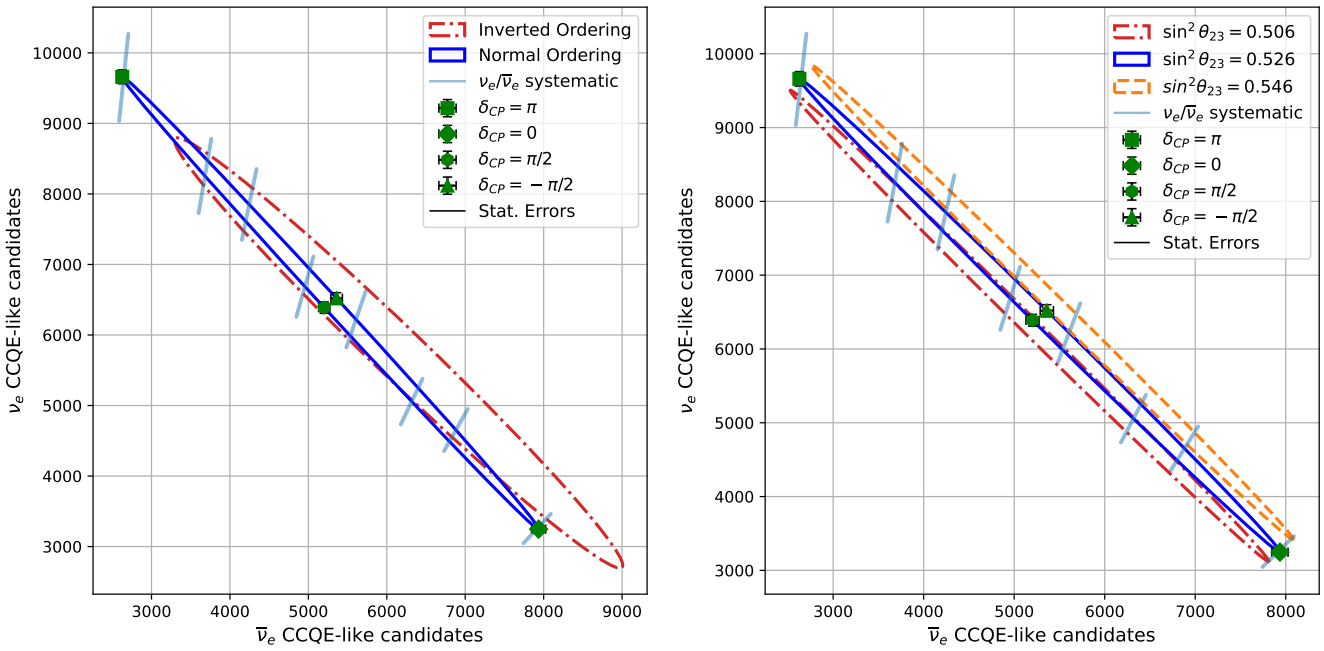

FIG. 7: The bi-event ellipse plots are shown for for the ESSνSB conceptual experiment using an FD baseline of 360 km. Left: bi-event ellipse for NO (blue solid line) and IO (red dashed line) and different values of δ_{CP}. Right: bi-event ellipse $\sin^2\theta_{23} = 0.506$ (red dashed line), 0.526 (blue solid line), 0.546 (orange dashed line) and δ_{CP}. The green dots highlight different values of δ_{CP} and the black bars show the corresponding statistical uncertainty. The diagonal light blue bar shows the modelling uncertainty on the $\nu_e/\bar{\nu}_e$ ($\Delta^{HF-CRPA/SF}_{\nu_e/\bar{\nu}_e}$).

small relative to the differences between any HF-CRPA or SuSAv2 configuration to SF or LFG. The regions of the phase space affected by relatively large model differences were found either at neutrino energies below 0.3 GeV for forward-going leptons, or around 0.6 GeV for leptons produced with angles larger than 100° with respect to the neutrino direction.

It is worth noting that the reported study adopts, for simplicity, a single systematic uncertainty per ratio considered to account for the difference between models over the whole kinematic phase space. However, more detailed studies will have to be performed in the future in order to also evaluate the impact of a systematic uncertainty affecting the modelling of the electron neutrino cross section as a function of the phase space and, consequently, to comprehensively estimate its impact on the measurement of the neutrino oscillation parameters. This will be particularly relevant in the case of analyses aiming to make precision measurements of δ_{CP} close to CP-violating values, or attempts to distinguish small from zero CP violation, where spectral shape information is particularly important. Nevertheless, in general, robust integrated uncertainties on the ratios, as presented here, remain most important for analyses focusing only on a discovery of CP-violation.

Although the uncertainty derived from the cross-section model spread is significant, there is scope to reduce it with both future theoretical developments and experimental measurements. In particular, precise measurements of muon neutrino interactions may be able to exclude particular modelling choices and specialised measurements may be able to provide a means to infer the electron neutrino cross section as a translation of a measured muon neutrino interactions. For example, is possible that measurements which are precisely sensitive to the CCQE muon neutrino cross section as function of lepton kinematics and neutrino energy may permit a useful inference of the electron neutrino cross section. Such a measurement of cross-section evolution as a function of neutrino energy may be possible using data collected at different off-axis angles with respect to the incoming neutrino beam [13, 45, 46].

Dedicated measurements of electron neutrino cross sections may also be very important, offering an opportunity to make direct constraints on the electron-to-muon neutrino cross section at near detectors. These measurements will involve analysing neutrino interactions from the small (∼1%) electron neutrino contamination to the primary muon neutrino flux at experiment's ND, attempts at which are often undermined by challenging backgrounds from photon-producing processes in muon neutrino interactions [47]. The ND electron neutrino flux also usually differs in shape from the muon neutrino flux or the electron neutrino appearance flux at the FD, and so high-statistics, high-purity measurements may be needed to isolate the relevant regions of phase

space. Hence, in order to perform such measurements, massive (several tonnes) ND that combine particle tracking and calorimetry capabilities [48, 49] would be desirable at the future LBL neutrino oscillation experiments to reduce the total uncertainty on the electron neutrino cross section down to a few percent. Partially because of this, the Hyper-K, DUNE, and ESSνSB experiments are planning for the installation of significantly more massive or performant NDs than T2K and NOvA. Additionally, the proposed NuStorm [50] project may facilitate high-statistics low-background measurements of electron neutrinos with a tuneable neutrino beam energy and specialised measurements of electron scattering may permit uncertainty reduction through model rejection at relevant kinematics.

The studies in this paper have been focused on CCQE interactions on an oxygen or carbon target. One may expect that effects analogous to those described in this article may be similar for an argon target, and so would be relevant to the neutrino beams of the Short-Baseline Neutrino (SBN) program at Fermilab [51], in particular to the lower energy off-axis NuMI beam seen by the ICARUS experiment [52]. Additionally, current and future oscillation experiments may benefit from additional theoretical investigations regarding analogous modelling differences in non-CCQE muon and electron neutrino cross-section ratios.

In conclusion, a detailed evaluation of uncertainties on the $\overset{(-)}{\nu}_e/\overset{(-)}{\nu}_\mu$ and $\nu_e/\bar{\nu}_e$ cross-section ratios from the modelling of nuclear effects at 0.2 to 1.2 GeV neutrino energies has been studied using the spread of predictions from a wide variety of models. Overall, it has been found that such uncertainties are unlikely to be dominant in measurements of the CP-violating $\sin\delta_{CP}$ term and neutrino mass ordering, although they may become crucial for analyses of $\cos\delta_{CP}$ and the $\sin^2\theta_{23}$ octant.

V. ACKNOWLEDGEMENTS

The authors would like to thank the T2K and Hyper-K collaborations, in particular for useful discussions in T2K's "Physics and Performance" and "Neutrino Interactions" working groups. The authors would like to thank Jan Sobczyk, Marco Martini, Claudio Giganti and Anna Ershova for their insightful comments on a draft version of the manuscript. SD would like to especially thank Kevin McFarland, Laura Munteanu and Callum Wilkinson for fruitful discussions. DS and TDi were supported by the Swiss National Science Foundation Eccellenza grant (SNSF PCEFP2_203261), Switzerland. TDe was supported by the Science and Technology Facilities Council (grant numbers ST/X002489/1, ST/V006215/1). LP is supported by a Royal Society University Research Fellowship (URF\R1\211661). Fermilab is operated by the Fermi Research Alliance, LLC under contract No. DE-AC02-07CH11359 with the United States Department of Energy.

[1] K. Abe et al. (T2K), Nature **580**, 339 (2020), [Erratum: Nature 583, E16 (2020)], arXiv:1910.03887 [hep-ex].
[2] K. Abe et al. (T2K), Phys. Rev. D **103**, 112008 (2021), arXiv:2101.03779 [hep-ex].
[3] M. A. Acero et al. (NOvA), Phys. Rev. Lett. **123**, 151803 (2019), arXiv:1906.04907 [hep-ex].
[4] M. A. Acero et al. (NOvA), (2021), arXiv:2108.08219 [hep-ex].
[5] Z. Maki, M. Nakagawa, and S. Sakata, Prog. Theor. Phys. **28**, 870 (1962).
[6] K. Abe et al. (T2K, J-PARC Neutrino Facility Group), (2019), arXiv:arXiv:1908.05141 [physics.ins-det].
[7] K. Abe et al. (Hyper-Kamiokande), (2018), arXiv:1805.04163 [physics.ins-det].
[8] R. Acciarri et al. (DUNE), (2015), arXiv:1512.06148 [physics.ins-det].
[9] A. Alekou et al., (2022), 10.1140/epjs/s11734-022-00664-w, arXiv:2206.01208 [hep-ex].
[10] L. Alvarez-Ruso et al., Prog. Part. Nucl. Phys. **100**, 1 (2018), arXiv:1706.03621 [hep-ph].
[11] K. Abe et al. (T2K), (2019), arXiv:1901.03750 [physics.ins-det].
[12] S. Manly, M. Kordosky, and O. behalf of the DUNE Collaboration, Instruments **5** (2021), 10.3390/instruments5040031.
[13] K. Abe et al. (Hyper-Kamiokande), (2018), arXiv:1805.04163 [physics.ins-det].
[14] M. Scott, PoS **ICHEP2020**, 174 (2021).
[15] A. Abed Abud et al. (DUNE), Instruments **5**, 31 (2021), arXiv:2103.13910 [physics.ins-det].
[16] M. Martini, N. Jachowicz, M. Ericson, V. Pandey, T. Van Cuyck, and N. Van Dessel, Phys. Rev. C **94**, 015501 (2016), arXiv:1602.00230 [nucl-th].
[17] M. Martini, M. Ericson, G. Chanfray, and J. Marteau, Phys. Rev. C **80**, 065501 (2009), arXiv:0910.2622 [nucl-th].
[18] N. Jachowicz, K. Heyde, J. Ryckebusch, and S. Rombouts, Phys. Rev. C **65**, 025501 (2002).
[19] A. M. Ankowski, Phys. Rev. C **96**, 035501 (2017), arXiv:1707.01014 [nucl-th].
[20] A. Nikolakopoulos, V. Pandey, J. Spitz, and N. Jachowicz, Phys. Rev. C **103**, 064603 (2021), arXiv:2010.05794 [nucl-th].
[21] J. Nieves and J. E. Sobczyk, Annals Phys. **383**, 455 (2017), arXiv:1701.03628 [nucl-th].
[22] A. Nikolakopoulos, N. Jachowicz, N. Van Dessel, K. Niewczas, R. González-Jiménez, J. M. Udías, and V. Pandey, Phys. Rev. Lett. **123**, 052501 (2019), arXiv:1901.08050 [nucl-th].
[23] A. Nikolakopoulos, R. González-Jiménez, N. Jachowicz, K. Niewczas, F. Sánchez, and J. M. Udías, Phys. Rev.

C **105**, 054603 (2022), arXiv:2202.01689 [nucl-th].
[24] R. González-Jiménez, A. Nikolakopoulos, N. Jachowicz, and J. M. Udías, Phys. Rev. C **100**, 045501 (2019), arXiv:1904.10696 [nucl-th].
[25] M. Day and K. S. McFarland, Phys. Rev. D **86**, 053003 (2012), arXiv:1206.6745 [hep-ph].
[26] O. Tomalak, Q. Chen, R. J. Hill, and K. S. McFarland, Nature Commun. **13**, 5286 (2022), arXiv:2105.07939 [hep-ph].
[27] O. Tomalak, Q. Chen, R. J. Hill, K. S. McFarland, and C. Wret, Phys. Rev. D **106**, 093006 (2022), arXiv:2204.11379 [hep-ph].
[28] K. Abe et al. (T2K), Phys. Rev. Lett. **124**, 161802 (2020), arXiv:1911.07283 [hep-ex].
[29] S. Dolan, A. Nikolakopoulos, O. Page, S. Gardiner, N. Jachowicz, and V. Pandey, Phys. Rev. D **106**, 073001 (2022), arXiv:2110.14601 [hep-ex].
[30] K. Abe et al. (T2K), Phys. Rev. D **101**, 112004 (2020), arXiv:2004.05434 [hep-ex].
[31] M. A. Acero et al. (NOvA), Phys. Rev. **D98**, 032012 (2018), arXiv:1806.00096 [hep-ex].
[32] B. Abi et al. (DUNE), Eur. Phys. J. C **80**, 978 (2020), arXiv:2006.16043 [hep-ex].
[33] Y. Hayato and L. Pickering, (2021), 10.1140/epjs/s11734-021-00287-7, arXiv:2106.15809 [hep-ph].
[34] J. Nieves, I. Ruiz Simo, and M. J. Vicente Vacas, Phys. Rev. **C83**, 045501 (2011), arXiv:1102.2777 [hep-ph].
[35] B. Bourguille, J. Nieves, and F. Sánchez, JHEP **04**, 004 (2021), arXiv:2012.12653 [hep-ph].
[36] O. Benhar, A. Fabrocini, S. Fantoni, and I. Sick, Nucl. Phys. **A579**, 493 (1994).
[37] P. Stowell et al., JINST **12**, P01016 (2017), arXiv:1612.07393 [hep-ex].
[38] R. Gonzaléz-Jiménez, G. D. Megias, M. B. Barbaro, J. A. Caballero, and T. W. Donnelly, Phys. Rev. C **90**, 035501 (2014), arXiv:1407.8346 [nucl-th].
[39] V. Pandey, N. Jachowicz, T. Van Cuyck, J. Ryckebusch, and M. Martini, Phys. Rev. C **92**, 024606 (2015), arXiv:1412.4624 [nucl-th].
[40] S. Dolan, G. D. Megias, and S. Bolognesi, (2019), arXiv:1905.08556 [hep-ex].
[41] C. Andreopoulos et al., Nucl. Instrum. Meth. A **614**, 87 (2010), arXiv:0905.2517 [hep-ph].
[42] F. Rademakers, R. Brun, P. Canal, et al., "ROOT - An Object-Oriented Data Analysis Framework. root-project/root: v6.10/04," (2017).
[43] C. Wilkinson et al., Phys. Rev. D **93**, 072010 (2016), arXiv:1601.05592 [hep-ex].
[44] M. Freund, Phys. Rev. D **64**, 053003 (2001), arXiv:hep-ph/0103300.
[45] S. Bhadra et al. (nuPRISM), (2014), arXiv:1412.3086 [physics.ins-det].
[46] DUNE Collaboration, (Near detector conceptual design report, in preparation).
[47] K. Abe et al. (T2K), JHEP **10**, 114 (2020), arXiv:2002.11986 [hep-ex].
[48] P. Abratenko et al. (MicroBooNE), Phys. Rev. Lett. **128**, 241801 (2022), arXiv:2110.14054 [hep-ex].
[49] A. Blondel et al., JINST **13**, P02006 (2018), arXiv:1707.01785 [physics.ins-det].
[50] L. A. Ruso et al. (nuSTORM), in 2022 Snowmass Summer Study (2022) arXiv:2203.07545 [hep-ex].
[51] P. A. Machado, O. Palamara, and D. W. Schmitz, Ann. Rev. Nucl. Part. Sci. **69**, 363 (2019), arXiv:1903.04608 [hep-ex].
[52] R. Howell, M. Betancourt, and B. Howard, (2020), 10.2172/1637617.
[53] K. Abe et al. (T2K), Phys. Rev. **D87**, 012001 (2013), [Addendum: Phys. Rev.D87,no.1,019902(2013)], arXiv:1211.0469 [hep-ex].
[54] `http://t2k-experiment.org/wp-content/uploads/T2Kflux2016.tar`, accessed: 07/12/2022.
[55] `https://github.com/rogerwendell/Prob3plusplus`, accessed: 07/12/2022.
[56] A. Rohatgi, "Webplotdigitizer: Version 4.6," (2022).

Appendix A: Simulation of experimental configurations

The method adopted to simulate and compute the neutrino interaction spectra for is described for both the Hyper-K and ESSνSB experimental configurations.

Hyper-K simulation: An experiment corresponding to ten years of data taking with a 187 kt of water target and an antineutrino beam mode exposure three times larger than the neutrino one, as reported in [13], is simulated with the NEUT neutrino event generator using the SF CCQE cross-section model and the T2K/Hyper-K flux [53, 54]. The Prob3++ software was used to calculate the neutrino oscillation probabilities [55] and, for a given set of oscillation parameter values, the number of expected events was computed as:

$$N_{osc}(E_\nu) = \sum_{E_\nu} \Phi(E_\nu) \times \sigma(E_\nu) \times N_{tgts} \times N_{POT} \times P_{osc}(E_\nu) \tag{A1}$$

where E_ν is the neutrino energy, Φ is the incoming neutrino flux (before oscillations occur), σ is the interaction cross section, N_{tgts} is the number of target nuclei, N_{POT} is the number of accelerator protons on target (POT) and P_{osc} is the oscillation appearance probability, either $\nu_\mu \to \nu_e$ for electron neutrino events or $\bar{\nu}_\mu \to \bar{\nu}_e$ for electron antineutrino events. Since N_{osc} corresponds to the expected number of CCQE events without considering detector efficiencies, smearing effects or background, the resulting total number of events is slightly different from the numbers reported in [13].

ESSνSB simulation: A method analogous to the one adopted for the Hyper-K simulation was used but using the neutrino and antineutrino flux distributions of the ESSνSB concept experiment. The fiducial active mass was taken to be 200 kt. The flux at a baseline of 100 km was obtained from the ESSνSB CDR [9] using a plot-digitizer [56]. It is then additionally scaled to a FD baseline of 360 km, assuming a radial broadening ($\sim 1/r^2$) of the beam. The neutrino and antineutrino oscillated CCQE event distributions predicted by the NEUT SF model are shown in fig. 8, using the same nominal oscil-

lation parameters as in section III and a baseline of 360 km.

The peak is at a lower energy and spans a wider range of angles with respect to the Hyper-K case, especially for antineutrinos. Given that there are more events in the region of kinematic phase space shown in fig. 1 to be susceptible to variations of R_{ν_e/ν_μ}, it is unsurprising that a larger uncertainty is found for ESSνSB compared to the Hyper-K experiment, as discussed in section III B.

Appendix B: Statistical Uncertainties

The SF and LFG model predictions where extracted using a NEUT monte-carlo simulation and are thus subject to a statistical uncertainty related to the number of events generated. For this analysis, 300 million events where produced per neutrino flavour and model. However, even with large numbers of events, the statistical uncertainty on cross-section ratios (or double ratios) is important to consider. The relative statistical uncertainty on a cross-section ratio can be calculated as:

$$\delta(E_\nu,\theta)/\left(N_A/N_B\right) = \sqrt{1/N_A(E_\nu,\theta) + 1/N_B(E_\nu,\theta)}, \tag{B1}$$

where N_A and N_B are the number of events within some bin of E_ν, θ of one of the flavours. Fig. 9 shows the relative statistical uncertainty on the cross-section ratios considered within this article, using the two dimensional binning shown in the majority of figures (10 degree bins in θ and 100 MeV bins in E_ν). Whilst the statistical uncertainty within individual bins shown can be up to ∼10%, it is usually at the ∼0-3% level in the regions of interest for this article.

When double ratios are considered (i.e. in the ratio of model predictions of two cross section ratios) the statistical uncertainty enters four times when comparing two NEUT-generated models (note that the calculations from the hadron tensor tables are analytical and have no statistical uncertainty). The size of the relative uncertainty on the double ratios of NEUT cross sections are also shown in fig. 9, reaching ∼20% for some bins at very high energies and angles but is generally less than ∼5% in regions of interest for this article.

Overall, it must be noted that the relative statistical uncertainly on the systematic uncertainties calculated within this article, which considers the entire integrated phase space, will be much smaller than the uncertainty on individual bins.

Appendix C: Pauli Blocking

A comparison of the cross section predicted by NEUT's SF model with and without Pauli blocking is shown in fig. 10. It is clear that the only region of the phase space affected by Pauli blocking is at low neutrino energies and forward lepton angle, where the ν_μ ($\bar{\nu}_\mu$) cross section becomes lower than the ν_e ($\bar{\nu}_e$) one. This region is also affected by a relatively large deviation from unity in $RR^{\text{SF / (SF w/o PB)}}_{\nu_e/\nu_\mu}$. However, this is also a region of very low cross section in all models and so barely overlaps with the distribution of events expected at the Hyper-K or ESSνSB FDs.

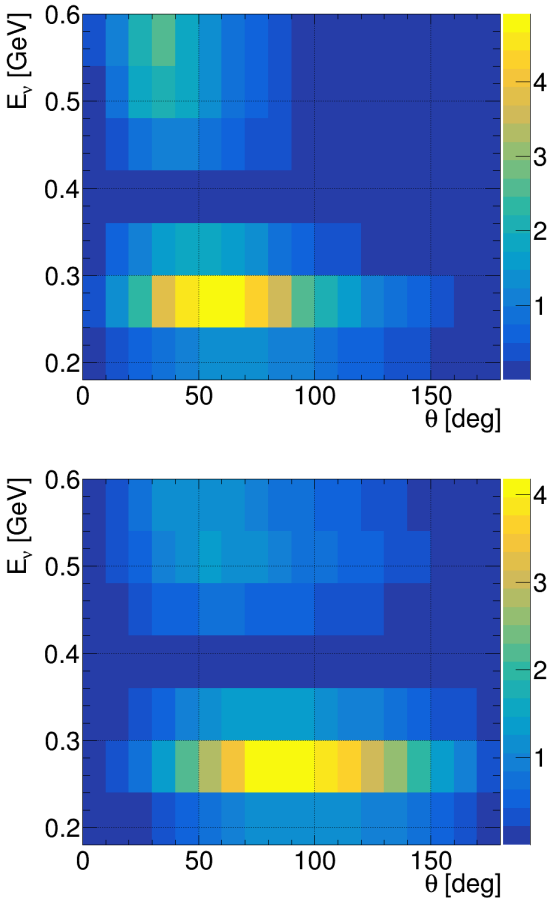

FIG. 8: The digitised ESSνSB oscillated NEUT SF-based event rates for ν_μ (left) and $\overline{\nu}_\mu$(right) expected at the dar detector. The X and Y axes show respectively the outgoing lepton angle and the neutrino energy. The Z-axis shows the relative proportion of the event rate in each bin as a percentage.

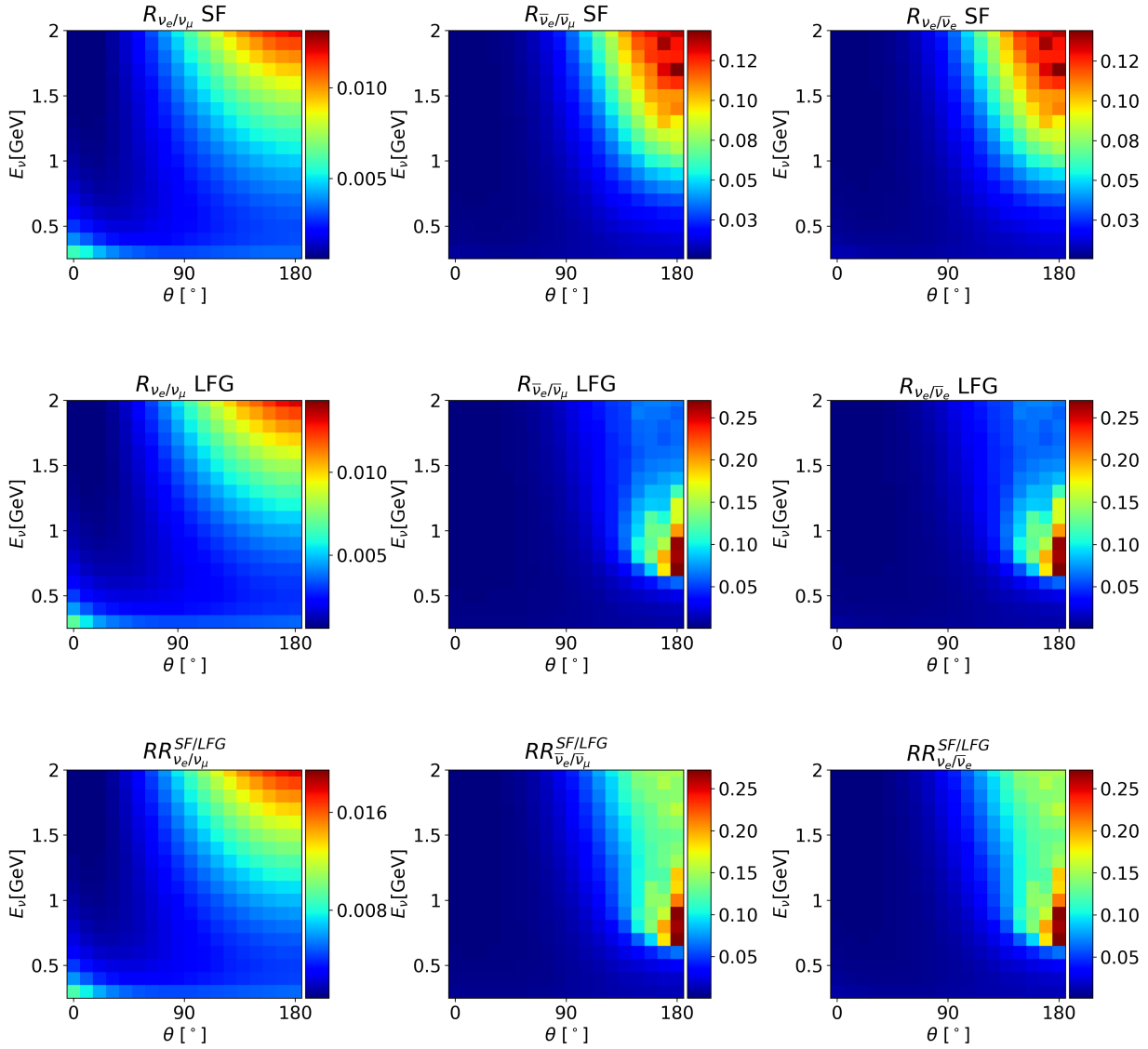

FIG. 9: The relative fractional statistical uncertainty on single ratio, eq. (1), and double ratio, eq. (2), for the SF and LFG models.

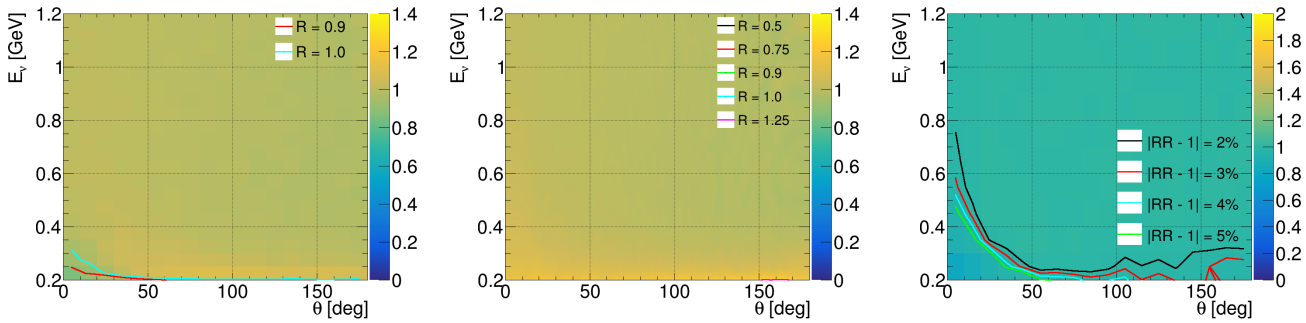

FIG. 10: $R^{\mathrm{SF}}_{\nu_e/\nu_\mu}$ (left), $R^{\mathrm{SF\ w/o\ PB}}_{\nu_e/\nu_\mu}$ (centre) and $RR^{\mathrm{SF\ /\ (SF\ w/o\ PB)}}_{\nu_e/\nu_\mu}$ (right) are shown. The double ratio of those two first plots is shown on the right. The contour lines highlight the regions where the single ratio significantly deviates from unity and are built using a bi-linear interpolation based on the four nearest bin centres [42]. Note that this uses unseen bins for neutrino energies less than 0.2 GeV.